MTLA 31 (2023) 101862

Contents lists available at ScienceDirect

Materialia

journal homepage: www.elsevier.com/locate/mtla

Full Length Article

A statistical analysis of the second 'pop-in' behaviour of the spherical-tip nanoindentation of Zr-based bulk metallic glasses

Priyanka Saini [a], Shankha Nag [b], Jae-il Jang [c], In-Chul Choi [d], Upadrasta Ramamurty [e,f], R.L. Narayan [a,*]

[a] Department of Materials Science and Engineering, Indian Institute of Technology, Delhi 110016, India
[b] Materials Modelling Division, Technical University of Darmstadt, Darmstadt 64206, Germany
[c] Division of Materials Science and Engineering, Hanyang University, Seoul 04763, the Republic of Korea
[d] School of Materials Science and Engineering, Kumoh National Institute of Technology, Gumi 39177, the Republic of Korea
[e] School of Mechanical and Aerospace Engineering, Nanyang Technological University, 639798 Singapore
[f] Institute of Materials Research and Engineering, Agency for Science, Technology and Research, Singapore 138634, Republic of Singapore

ARTICLE INFO

Keywords:
Metallic glass
Plastic deformation
Nanoindentation
Statistics
Shear bands

ABSTRACT

Statistical analyses of the shear stresses, τ_y, at which the first 'pop-ins' occur during the spherical tip nanoindentation of a wide variety of materials is often conducted to understand the micromechanisms of incipient plasticity. In an earlier paper, we reported such a study on data generated on several different Zr-based bulk metallic glasses (BMGs) using a wide range of experimental variables, such as the tip radius, R_i, loading rate, $\dot{P}$, and structural state of the glass. In the present work, we analyse the second pop-in stress, τ_2, data employing the expectation maximization algorithm in conjunction with the Akaike Information Criterion to examine which of the single and mixed (bimodal) versions of the Gaussian, Lognormal and Weibull (both 2 and 3 parameter) statistical models best describes the stochasticity of τ_2. Results show that the 3-parameter Weibull distribution also captures the stochasticity of τ_2, just as it does for τ_y. For datasets of τ_2 that are generated with larger R_i and $\dot{P}$, the bimodal 3-parameter Weibull distribution is a better descriptor of the dispersion. While Weibull exponent, m, of τ_2 datasets is marginally higher than that of τ_y, their kernel density estimates (KDEs) are similar. However, there is a relative shift of the KDEs of τ_2 to smaller values compared to that of τ_y. From mechanistic arguments, τ_2 is determined as the stress to nucleate a second shear band over a previously formed shear band and its stochasticity is attributed solely to the mechanical heterogeneity of the material within it. On this basis, the average shear strength of the shear band is estimated to be ~8–11% and 15–17% lower than the strength of the undeformed BMG in the as cast condition and structurally relaxed conditions, respectively. This study provides an understanding of how plasticity develops in BMGs during nanoindentation.

1. Introduction

The local shear yield strength, τ_y, of bulk metallic glasses (BMGs) is measured from the load at which the first pop-in occurs, P_{FP}, in the load (P) vs. displacement (h) curve, during spherical-tip nanoindentation. Owing to the disordered nature of packing of atoms in BMGs, τ_y exhibits significant heterogeneity, the statistical analysis of which has been utilized to extract quantitative and qualitative information on the microscopic carriers of plasticity in the material [1–6]. Packard et al. [7] calculated the cumulative distribution function (CDF) of the τ_y data generated on single crystal platinum and 3 different BMGs and observed that the nanoscale dispersion in strength is affected by both thermal fluctuations as well as structural heterogeneities in BMGs. Choi et al. [8, 9] combined the functional form of the CDF of τ_y with the cooperative shear model (CSM) proposed by Johnson and Samwer [10] to calculate the activation volume and the average size of a shear transformation zone (STZ), which is the widely accepted unit carrier of plasticity in BMGs. Perepezko et al. [2] obtained a statistical fit for τ_y data with a bimodal Gaussian distribution and concluded that there are two distinct types of defects that can trigger the formation of an incipient shear band at different stresses.

Nag et al. [1] critically examined the work of Perepezko et al. and

* Corresponding author.
E-mail address: rlnarayan@iitd.ac.in (R.L. Narayan).

https://doi.org/10.1016/j.mtla.2023.101862
Received 20 June 2023; Accepted 27 July 2023
Available online 28 July 2023

noted that instead of implicitly assuming that τ_y data will be best fit by a Gaussian distribution, it is important to identify the distribution that best describes τ_y data, amongst different candidate distributions. For this, they first analysed the τ_y data with unimodal and bimodal versions of Gaussian, lognormal, and Weibull distributions by employing maximum likelihood estimates (MLEs). Then, by applying the Akaike information criterion (AIC) for each model, they firmly established that the dispersion in τ_y is described best by the 3-parameter Weibull (3 W) distribution. Weibull statistics is widely used for assessing the strength variability of brittle materials, where failure initiates at the largest defect, as it acts as the 'weakest link' in the material [11]. Likewise, Nag et al. [1] argued that the variations in τ_y are justifiably described by the Weibull distribution as yielding in BMGs also initiates at structural weak links, which are regions with lower atomic packing. They observed that τ_y has a bimodal distribution when indenters with large radii are used or when the loading rates of the test are relatively higher. They suggested that in both these situations, the bimodality of the τ_y distribution is an outcome of the availability of multiple shear band paths that operate at different stresses.

While most studies have hitherto only focussed on the statistics of incipient plasticity during indentation of BMGs, none have addressed the evolution of plasticity beyond the yield point. In crystalline materials, the dispersion in the first and second pop-in stresses is characterized by the Gaussian and power law statistics, respectively [12]. This change is attributed to the transition in deformation mechanism from dislocation nucleation during yielding to dislocation network evolution with increasing plastic strain [12]. In BMGs, both first and second pop-in stresses are expected to correspond to the operation of a shear band. This raises the following questions pertaining to the statistical nature of the stress, τ_2, associated with the second pop-in during spherical-tip nanoindentation experiments on BMGs. First, would τ_2 exhibit dispersion? If yes, what would be the statistical nature of it? Second, what are the characteristics of this dispersion compared to that of τ_y, i.e., is the dispersion in τ_2 more narrower or wider than the latter? Finally, once the most appropriate distribution is identified, can a correlation with the mechanism of subsequent shear band formation and the distribution of shear stress be established?

To answer the above questions, we performed a detailed statistical analysis on 14 datasets of τ_2 that were generated by varying experimental variables such as structural state of the BMG, indenter radius, R_i, and loading rate, $\dot{P}$, which were also the reference datasets for Nag et al. [1]. For determining the appropriate distribution that describes these datasets, the statistical analyses procedures employed by Nag et al. [1] were utilized. Results show that the observed scatter in τ_2 is best described by the 3 W distribution, which is similar to that seen for τ_y distributions, with minor differences. These differences are linked to the change in the conditions required for the nucleation of a shear band during incipient plasticity and that after a shear band has already formed. Further analysis of the kernel density estimates (KDEs) of τ_y and τ_2 datasets provides a lower bound estimate of the shear strength of shear bands.

2. Materials and experiments

Table 1 provides a summary of the 14 experimental datasets of several indentation experiments, which were performed on two different Zr-based MGs with the nominal compositions of $Zr_{35}Ti_{30}Cu_{8.25}Be_{26.75}$ and $Zr_{52.5}Cu_{17.9}Ni_{14.6}Al_{10}Ti_5$ (commercially referred to as Vit 105) with T_g of 578 and 673 K, respectively. Details of their processing and fabrication are listed elsewhere [13–15]. These alloys were tested at room temperature (~300 K) in as-cast (AC), intermediately annealed (A) and structurally relaxed (SR) states (see Table 1 for the annealing conditions employed). The A and SR states were attained by annealing the MG samples at temperatures 40 degrees above/below their T_g. For all datasets, nanoindentation experiments were performed

Table 1
Summary of the metallic glass alloy compositions, their structural states and indentation parameters (loading rate, $\dot{P}$, indenter radius, R_i) utilized in this study. The size of the SR1 dataset was found to be insufficient for performing statistical analyses.

Dataset	Composition	Thermal history	$\dot{P}$ (mN/s)	R_i (μm)	Data size for 2nd pop-ins
AC1	$Zr_{52.5}Cu_{17.9}Ni_{14.6}Al_{10}Ti_5$ (T_g = 673 K)	As-cast	1	31.5	100
AC2	"	As-cast	5	31.5	81
AC3	"	As-cast	10	31.5	65
AC4	"	As-cast	20	31.5	98
AC5	"	As-cast	1	5.75	120
AC6	"	As-cast	1	2.91	100
AC7	$Zr_{35}Ti_{30}Cu_{8.25}Be_{26.75}$ (T_g = 578 K)	As-cast	0.4	1	76
A1	"	Annealed, 553 K, 520 min	0.4	1	76
A2	"	Annealed, 573 K, 170 min	0.4	1	80
A3	"	Annealed, 593 K, 41 min	0.4	1	66
A4	"	Annealed, 613 K, 15 min	0.4	1	70
SR1	$Zr_{52.5}Cu_{17.9}Ni_{14.6}Al_{10}Ti_5$ (T_g = 673 K)	Annealed, 630 K, 60 min	1	5.75	41
SR2	"	Annealed, 630 K, 60 min	1	2.91	56
SR3	$Zr_{35}Ti_{30}Cu_{8.25}Be_{26.75}$ (T_g = 578 K)	Annealed, 558 K, 1440 min	0.4	1	80

on mirror-polished specimens using a Hysitron Triboindeter which is equipped with spherical indenter tips of different radii (R_i = 1, 2.91, 5.75 and 31.5 μm). Polishing was performed with diamond suspension sprayed over a cloth on a rotating disk polishing machine and kerosene was continuously added to minimize heating of the sample due to friction.

For other datasets, the details of R_i and loading rates, $\dot{P}$, that were employed for performing these testsare mentioned in Table 1. During spherical indentation, the maximum shear stress underneath the indenter, τ_{max}, at any given load, P, is given by [16,17]:

$$\tau_{max} = 0.17\left(\frac{E_r}{R_i}\right)^{2/3} P^{1/3} \tag{1}$$

where E_r is reduced modulus, given by

$$\frac{1}{E_r} = \frac{1-\nu_s^2}{E_s} + \frac{1-\nu_i^2}{E_i} \tag{2}$$

where E and ν are the elastic modulus and Poisson's ratio, with the subscripts 's' and 'i' indicating the sample and the indenter, respectively. A schematic illustration of the nanoindentation test is shown in Fig. 1(a) and the representative P-h curve is shown in Fig. 1(b), wherein P_{FP} and P_{SP} indicate the points at which the first and second displacement bursts are observed, respectively. These bursts are differentiated from the noise, by studying the variations of the indenter velocity (dh/dt) during the test. Fig. 1(c) displays dh/dt profile as a function of P. Several small spikes in dh/dt are observed, which are classified as noise due to vibration of the tip. However, the significantly larger peaks are identified as displacement bursts or pop-ins [18].

The load, P_{FP}, at which first pop-in (FP) occurs corresponds to the

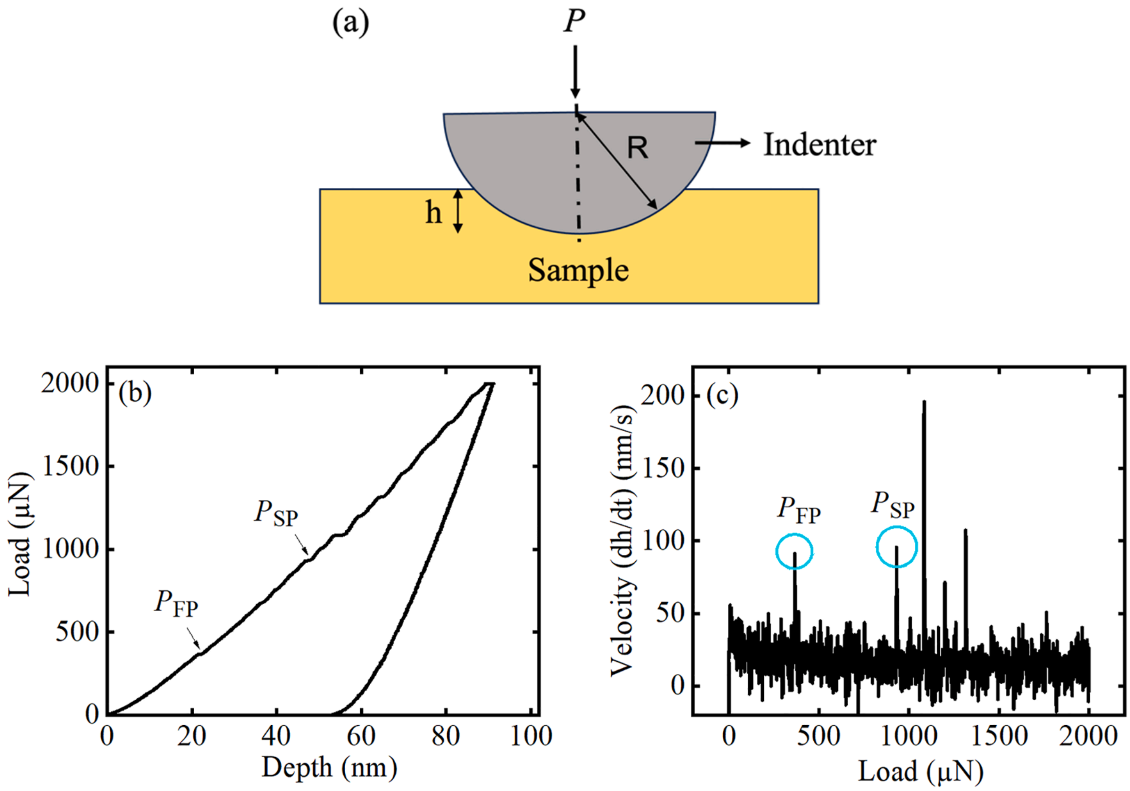

Fig. 1. (a) Schematic illustration of the nanoindentation test, (b) A representative *P-h* curve on a BMG showing first two pop-ins occurring in the loading segment of the curve and (c) corresponding velocity profile; blue circles indicate velocity spikes.

point where P, vs. depth of penetration, h, curve deviates abruptly from that predicted by the Hertzian elastic contact mechanics (see Fig. 1(b)). Each subsequent displacement excursion represents a discrete plastic event, where a shear band is formed in the material and is accompanied by strain relaxation in the rest of the material. Therefore, each pop- in the *P-h* curve of a BMG can be treated as a discrete plastic event. At P_{FP}, which is the first plastic event, τ_{max} corresponds to the local shear yield strength, τ_y. Similarly, τ_{max} at P_{SP} is the shear stress, τ^{SP} that represents the second plastic event. Unlike τ_y, which represents the stress that triggers incipient plasticity, τ^{SP}, is not the actual stress at which the second plastic event is initiated. This is because there is some stress relaxation after the first pop-in, which causes a drop in the mean contact pressure, p_m, and hence τ_{max}, during the first pop-in. This stress drop must be considered for calculating the actual maximum shear stress corresponding to the second plastic event. For this, the drop in p_m, Δp_m, can be first calculated from the Hertzian contact relation (see also S1 in SI),

$$\Delta p_m = \frac{4}{3\pi}\frac{E_r}{R_i^{1/2}}(\Delta h)^{1/2} \tag{3}$$

where Δh is the magnitude of the first pop-in displacement. Then, using the relation (see S1 in SI),

$$\tau_{max} \sim 0.47 p_m \tag{4}$$

the drop in maximum shear stress, $\Delta\tau_{max}$, can be calculated. Finally, the actual maximum shear stress for initiating the second plastic event is calculated from,

$$\tau_2 = \tau^{SP} - \Delta\tau_{max} \tag{5}$$

Pop-in events beyond the 2nd were not studied as the number of such occurrences were insufficient for performing a valid statistical analysis.

3. Statistical analyses

3.1. Statistical models

As already mentioned, Nag et al.'s study shows that 3 W model are the best descriptors of τ_y data in BMGs [1]. However, since it is not obvious that the 3 W model would also best describe τ_2 data, the following statistical models were again considered in evaluating its dispersions. Gaussian (G) model was chosen as a candidate model as it is the most commonly used statistical model to fit most experimental data, although it has an intrinsic limitation in the present context that a normally distributed random variable can also take negative values, whereas τ_y and τ_2 are always positive. Both Lognormal (LN) and W distributions do not have this drawback. LN approximates multiplicative degradation processes [19,20] and given that plasticity in MGs involves strain localization through the cascading activation of multiple STZ events [21], it is worth examining it as a possible candidate distribution.

Considering these three models, statistical analyses of the experimental τ_2 data was performed. Both two- and three- parameter versions of the W distribution, which are abbreviated as 2 W and 3 W, respectively, are examined. For the G and LN distributions, the probability density functions (PDFs), f, are [22,23]

$$f(u) = \frac{1}{\sigma\sqrt{2\pi}} exp\left(\frac{-(u-\mu)^2}{2\sigma^2}\right) \tag{6}$$

$$f(u) = \frac{1}{u\sigma\sqrt{2\pi}} exp\left(\frac{-(lnu-\mu)^2}{2\sigma^2}\right), u > 0 \tag{7}$$

where u is the data, μ and σ are mean and standard deviation, respectively. In the case of 3 W distribution, f is given as,

$$f(u) = \begin{cases} \frac{m}{\beta}\left(\frac{u-\alpha}{\beta}\right)^{m-1} exp\left(-\left(\frac{u-\alpha}{\beta}\right)^{m}\right), u \geq 0 \\ 0, \ u < 0 \end{cases} \tag{8}$$

where α and β are location and scale parameters respectively, and m is the Weibull modulus. For 2 W distribution, $\alpha = 0$. The probability density function for two-component mixture models, f_M, is obtained from the weighted linear combination of f, which is,

$$f_M(u|p,\theta_1,\theta_2) = pf(u|\theta_1) + (1-p)f(u|\theta_2) \tag{9}$$

where p is the proportion of $f(u|\theta_1)$ and θ is the parameter space [1].

3.2. Sample size evaluation

Any statistical inference requires large (ideally infinite) data, which is not possible to generate in lab-scale experiments. Considering this, we first conducted sample size optimization tests for different statistical models examined in this study. The procedure for conducting these tests is listed in section S2.1 of the supplementary information (SI). From this, it was determined that a minimum sample size of 50 is sufficient for reliable and consistent inference. The data size of the second pop-ins are listed in Table 1. The data set that did not meet the above-mentioned sample size criteria (i.e. SR1) (Table 1) will henceforth not be considered.

3.3. Model selection

The maximum likelihood estimates (MLEs) are known to give best fit estimates with respect to consistency and rate of convergence, given certain regularity conditions are satisfied by the chosen model [22]. For bimodal distributions, the Expectation-Maximization Algorithm (EMA) was employed to estimate MLEs. Details of these procedures are provided in section S2.2 in SI and also discussed in Nag et al. [1].

Then, AIC [24] was utilized to assess the suitability of the selected model to describe the data. The values of AIC were computed using the following equation [25]:

$$AIC = -2lnL(\widehat{\theta}) + 2\gamma, \tag{10}$$

where γ is the number of parameters to be fitted in the model (see Table S1) and $L(\widehat{\theta})$ is the maximum likelihood. *The model that yields the lowest AIC for a given dataset is the best fitting model for that particular dataset.* See section S2.3 for further details on AIC.

4. Results

The sample sizes of most datasets of τ_2, with the exception of SR1, were found to be sufficient for performing valid statistical analyses. In Table 2, AIC estimates for these 13 datasets of τ_2, considering the chosen distributions in the study, are listed. For a given dataset, the model that yields the lowest AIC value is considered as its best descriptor (see Section S2.3 in SI for details). It is evident that AIC of the bimodal 3 W distribution yields the lowest value for AC1-AC4, with the exception in AC2, which is best described by bimodal 2 W while 3 W yields the next lowest value of AIC for it. For the remaining 9 datasets unimodal 3 W has the lowest AIC values.

Table 3 lists MLEs of the proportions of 3 W bimodal components and the p-values for bimodal and unimodal 3 W distributions for the 13 datasets. Apart from AC1-AC4 datasets, where both components are significant, in the other 10 datasets, one of the two components is > 91% while the other varies between 1 and 8%. Considering that sampling noise or experimental errors can lead to such small second components, it is reasonable to ignore them and conclude that the unimodal 3 W distribution effectively represents the stochastic nature of τ_2 in these 9 datasets, whereas bimodal 3 W distribution best describes that of AC1-AC4.

Next, τ_2 datasets are fit with these MLEs and the 'bootstrap method' of the Kolmogorov-Smirnov (KS) test was employed to test the goodness-of-fit of the uni- and bi-modal 3 W distributions [26,27] (See Section S2.4 in SI for details). The p-values for both the distributions are listed in Table 3. For all datasets, the p-values are higher than the chosen value of the significance level, $\alpha_s \sim 0.05$. This observation implies that neither model can be rejected only on the basis of goodness-of-fit. Note that the KS test is only appropriate for testing if the candidate models fit the experimental data well and should not be used for choosing the appropriate statistical model. AIC tests should be exclusively relied upon for model selection. From these observations, it can be inferred that the stochasticity of τ_2 is represented by the unimodal 3 W distribution, except in the cases of AC1-AC4 datasets, which are best described by the bimodal 3 W distribution.

Next, the specific characteristics of the distributions that describe these datasets are examined. The KDEs of τ_2 for all datasets are shown in Fig. 2. For AC1–AC4 datasets (see Fig. 2(a)), which are produced with a large indenter ($R_i = 31.5$ μm) but with varying $\dot{P}$, an increase in $\dot{P}$ from 5 mN/s to 10 mN/s, broadens the distribution, i.e., shifts the largest value of τ_2 distribution from 2.5 GPa to 3 GPa and increases its bimodality. Similarly, with decreasing R_i, τ_2 distributions shift to higher values (see Fig. 2(b)). In contrast, structural relaxation of the BMG narrows the distribution shifts the peak of the τ_2 distribution to higher values (see Fig. 2(c)).

Note that most of the inferences on the stochasticity of τ_2 are similar to those observed for τ_y by Nag et al. [1]. For instance, Nag et al. determined that the stochasticity of τ_y is best described by the 3 W bimodal distribution for AC1-AC4 datasets and by 3 W unimodal

Table 2
Akaike information criterion (AIC) estimates of τ_2. The estimates with the lowest value amongst all competing models for the respective dataset are highlighted in bold. G, LN, 2 W and 3 W refer to Gaussian, lognormal, two and three parameter Weibull distributions.

Dataset	Bimodal distribution				Unimodal distribution			
	G	LN	2W	3W	G	LN	2W	3W
AC1	19.75	19.97	20.99	**19.28**	20.03	24.04	19.32	19.38
AC2	−15.89	−15.46	**−21.62**	−21.52	−20.16	−16.92	−21.33	−20.04
AC3	43.86	44.06	47	**43.82**	69.49	61.94	77.24	50.52
AC4	41.44	41.48	51.46	**41.40**	58.73	63.57	54.76	56.74
AC5	67.44	64.68	70.48	62.28	66.91	60.28	76.44	**59.80**
AC6	109.52	109.84	109.26	108.24	113.5	107.5	123.2	**107.4**
AC7	42.72	42.76	42.2	42.84	39.29	43.38	40.12	**38.29**
A1	82.46	83.54	83.14	83.12	86.86	88.54	87.88	**81.61**
A2	108.16	108.1	108.98	104.52	106.81	109.79	106.73	**104.2**
A3	80.7	82.1	80.4	81.3	81.98	88.56	77.64	**77.61**
A4	76.72	78.72	77.58	71.3	74.19	73.94	78.78	**70.39**
SR2	−22.7	−22.6	−19.1	−26.62	−24.05	−26.58	−3.60	**−26.72**
SR3	109.24	109.56	110.24	102.5	104.12	104.96	107.84	**101.4**

Table 3
Maximum likelihood estimates (MLEs) and p-values of the KS test of unimodal and bimodal 3-parameter Weibull (3 W) distributions of τ_2.

Dataset	3 W Bimodal					3 W Unimodal			
	Proportion	α	β	m	p-value	α	β	m	p-value
AC1	0.35	1.27	0.42	1.93	0.98	0.97	1.01	3.96	0.82
	0.65	1.27	0.81	4.37					
AC2	0.41	1.13	0.99	7.28	0.89	0.85	1.03	5.54	0.74
	0.59	1.71	0.45	4.12					
AC3	0.48	1.26	1.13	4.29	0.99	1.46	0.59	1.49	0.55
	0.51	1.42	0.32	2.60					
AC4	0.58	1.09	2.53	16.59	0.99	0.46	2.79	8.97	0.23
	0.42	1.01	1.92	11.26					
AC5	0.96	1.39	0.63	2.69	0.99	1.45	0.80	1.86	0.98
	0.04	2.31	0.27	0.91					
AC6	0.02	1.67	0.01	2.01	0.65	1.59	1.01	2.17	0.72
	0.98	1.73	0.87	1.91					
AC7	0.97	0.23	0.59	2.91	0.72	0.25	0.58	2.69	0.94
	0.03	0.97	0.25	79.26					
A1	0.97	0.78	2.35	5.82	0.8	1.57	1.56	3.66	0.82
	0.03	3.61	0.06	235.69					
A2	0.96	0.33	2.77	6.19	0.97	1.47	1.61	3.51	0.91
	0.04	3.30	0.004	5.95					
A3	0.94	0.49	2.70	6.81	0.92	0.54	3.76	9.91	0.80
	0.06	1.58	1.84	310.83					
A4	0.03	0.32	2.18	462.95	0.99	1.99	1.16	2.82	0.99
	0.97	1.96	1.22	3.04					
SR2	0.98	2.41	0.99	3.72	0.89	2.51	0.57	2.61	0.76
	0.02	3.23	0.12	312.64					
SR3	0.01	2.13	0.09	217.32	0.99	1.94	1.64	3.27	0.99
	0.99	2.19	1.39	2.82					

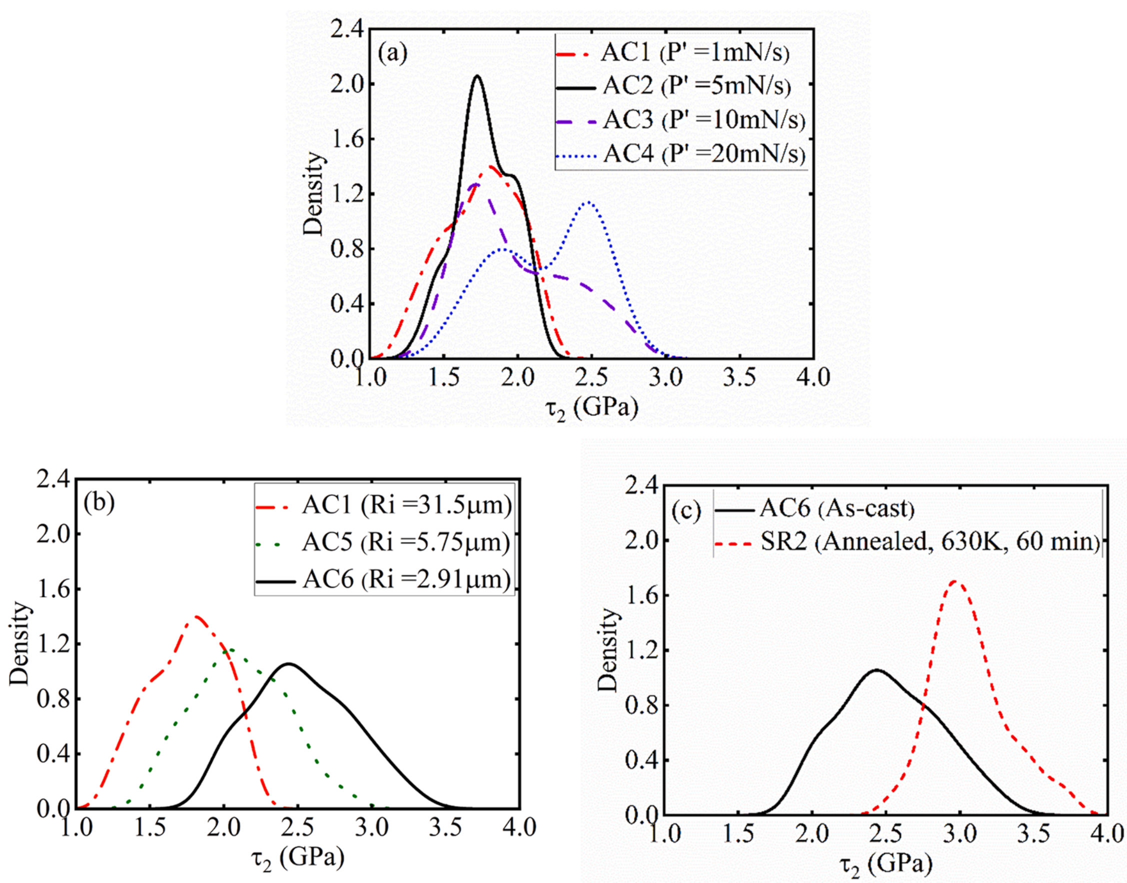

Fig. 2. Strength distribution represented as kernel density estimates (KDE) of τ_2 in 2nd pop-in of Zr-based BMGs demonstrating the effects of (a) loading rate ($\dot{P}$), (b) indenter tip radius, R_i and (c) thermal history.

distribution for other datasets [1]. It was also observed that for datasets produced with a large indenter (R_i = 31.5 μm) or at higher $\dot{P}$, the τ_y distribution shifts to higher values. Additionally, the τ_y distribution of the structurally relaxed BMG is narrower and its peak shifts to higher values compared to that of its as-cast counterpart.

To further compare the τ_2 and τ_y distributions, KDEs of some representative datasets are shown in Fig. 3. KDEs of τ_2 and τ_y for all other datasets are shown in Fig. S2. The widths of the KDEs of τ_2 and τ_y are similar but those of the latter are shifted to higher values compared to τ_2 distributions, which indicates that the second plastic event occurs at a lower stress than the first one. In Table S2, the range of τ_2 and τ_y values for all datasets are listed. From these, it is evident that the τ_y distributions have shifted to 15–17% higher values compared to that of τ_2 for SR2 and SR3, whereas for all other datasets the magnitude of the shift is only 8–11%.

Some additional differences in the distributions were identified when the characteristics of the two distributions are compared. For datasets AC1-AC4, *m* of both components of the τ_2 distributions are moderately higher than those of the τ_y distributions. For instance, *m* of one of the components of AC2 is ~7.3, whereas m of both components of AC4 datasets are 16.6 and 11.3, respectively, indicating a significant narrowing of the dispersions. Nag et al. [1] measured similarly high values of *m* for AC3 and AC4. In the datasets that are represented by the unimodal 3 W distribution, *m* is in the range of 1.8–3.6, with the exception of A3, which is slightly higher than those of τ_y, which in the range of 1.5–2.5 [1]. Given that magnitudes of *m* and scale with the skewness of the distribution, τ_2 distributions are only marginally more skewed than those of τ_y.

5. Discussion

5.1. Physical significance of 3 W distribution describing τ_2 data

In spherical tip indentation of BMGs, the first pop-in event, which signifies yielding, occurs when an embryonic shear band is nucleated underneath the indenter [28,29]. Shear bands form by the linking of shear transformation zones (STZs), which are present in regions with lower atomic packing fraction or greater free volume [27,30–35]. However, since there are stress gradients underneath a spherical indenter, an embryonic shear band can nucleate only along a shearing plane where a minimum number of STZs can be activated. On the premise that yielding initiates at the weakest link in the material, Nag et al. [1] established a physical basis for analysing τ_y data using the Weibull statistics, which is applicable to this study as well. It was also noted that the characteristics of the 3 W distribution for τ_y, obtained from indentation tests, are distinctly different than that for failure strength data, which is obtained from tension and compression tests on BMGs. This difference stems from the fact that there is a critical strain for shear localisation within a shear band that must be attained to cause failure in tension and compression [36,37]. In contrast, incipient plasticity in indentation is driven by the operation of STZs, whose energy barrier can exhibit a large variance [38–41].

Nag et al. [1] also addressed the effects of R_i and $\dot{P}$ on the parameters and bimodality of τ_y distributions. They noted that the volume of the material probed by the spherical indenter increases cubically with increase in R_i. This implies that an indenter with larger R_i can potentially activate several more STZs in a BMG than that with smaller R_i [1]. Since smaller tips have access to a lesser number of STZs, higher stress is

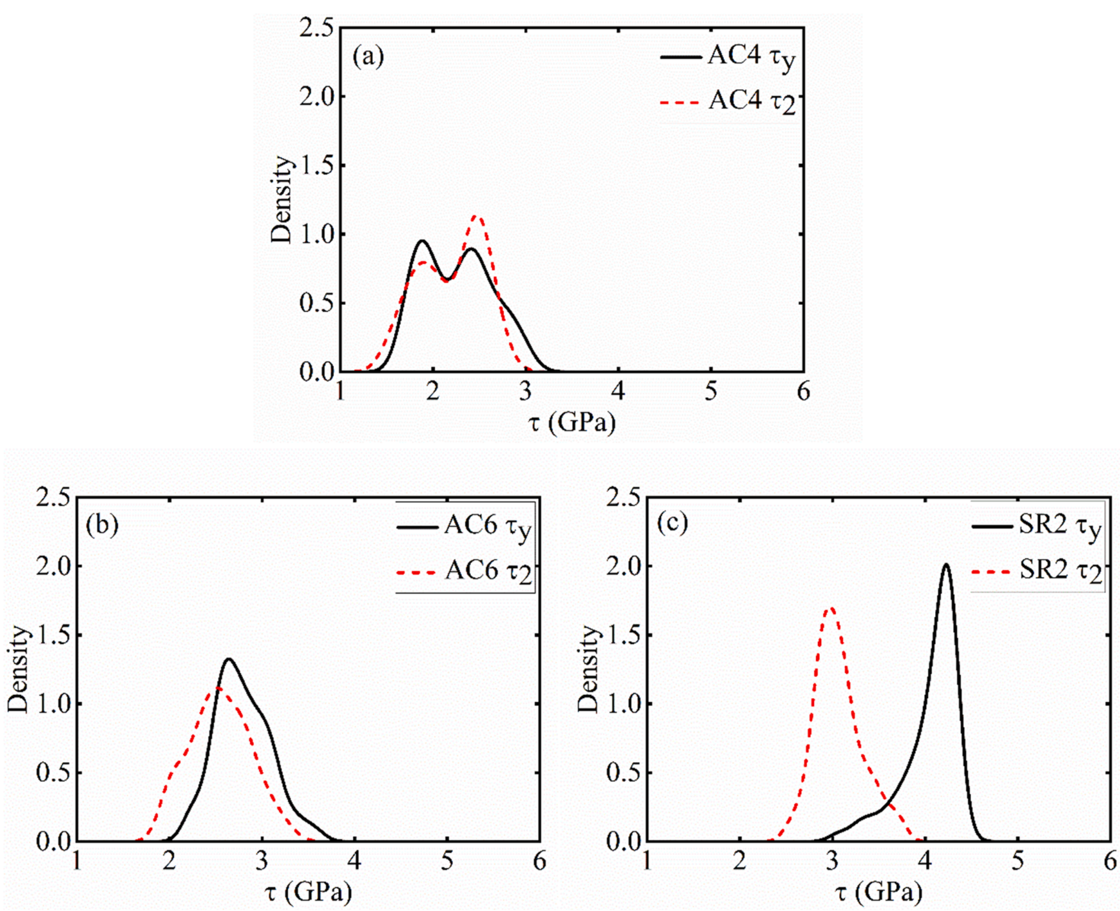

Fig. 3. Strength distributions represented as kernel density estimates (KDE) of 1st and 2nd pop-in events for Zr-based BMGs demonstrating the effects of (a) loading rate ($\dot{P}$), (b) indenter tip radius, R_i and (c) thermal history.

necessary for nucleating a shear band, which explains the observed shift in the τ_y distribution to higher values when indenters with smaller R_i are used. Also, owing to the fewer number of operable STZs in the deformed volume, the nucleation of multiple shear bands becomes unlikely. In contrast, when a tip with large R_i (~31.5 μm) is used, the availability of a larger number of STZs in the deformed volume enhances the likelihood of nucleating shear bands from multiple sources [40,41].

Besides this, Nag et al. [1] analysed the variations of τ_{max} underneath a spherical indenter using the Hertzian solutions for elastic contact between a sphere and a flat surface [16] and determined four 2-dimensional projections of shear planes where plasticity could potentially initiate. A plot of these τ_{max} contours is shown in Fig. 4, where the normalized coordinates, r' and z' represent the two-dimensional space for stress contours (see section S1 in SI for details). Nag et al. then established that a shear band can only form along the contour where the following two conditions are satisfied simultaneously. (i) A minimum critical value of the Mohr-Coulomb flow stress, τ_{MC}, is sustained over the τ_{max} contour [18]. (ii) The shear stress gradients, $\frac{\partial \tau_{MC}}{\partial x}$, along the trajectory are low [42–44]. Applying this criterion, they determined that when indenters with a smaller R_i (1 – 5 μm) are used, only shear paths around contour C (see Fig. 4) is the preferred path for shear band nucleation. Alternately, when indenters with large R_i are employed or when tests are performed at higher $\dot{P}$, regions encompassing both the contours C and D are favourable for shear band nucleation. Given that distinctly different stresses are required to nucleate a shear band along C and D contours, the τ_y distributions become bimodal. They also rationalized the shift in τ_y distribution to higher stresses after structural relaxation to the lack of free volume in the BMG, which raises the average stress required to nucleate shear bands [45–47].

With the above as the background, we interpret the results of the statistical analysis of the τ_2 data sets. At the outset, since τ_2 data is also described best by 3 W distributions, it is evident that any post-yield plastic event in BMGs will also be governed by deformation at the weakest link in the material. The atomic structure inside a shear band, owing to the accumulation of plastic strain, is more disordered and is, therefore, softer compared to the rest of the BMG [5]. As a consequence, once shear bands nucleate, plastic flow localizes within them, leading to the observed strain softening behaviour of BMGs [31]. Strain softening, which is the converse of strain hardening, localizes plastic flow within the deformed area, which in this case, is the existing shear band. The failure of tensile and compression specimens along a single shear band supports this argument [48]. This implies that the first shear band that forms in BMGs during yielding is likely to be the favoured site for the formation of subsequent bands. Moser et al. [28] performed Berkovich-tip nanoindentation experiments on BMGs and observed shear band formation in real time inside an SEM and reached a similar conclusion. Besides noting that each displacement burst in the *P-h* curve corresponds to the formation of a shear band, they observed that previously formed shear bands are the preferred (but not necessarily the only) nucleation sites for the formation of subsequent shear bands. The same is expected to hold true for the present study as it also involves nanoindentation, albeit with a spherical tip.

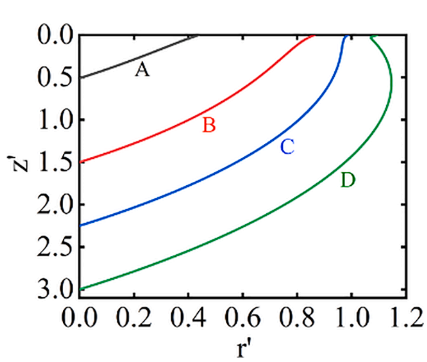

Fig. 4. Contours of τ_{max} in the material calculated from the Hertzian contact relations for a sphere in elastic contact with a flat surface.

Considering that a new shear band forms along the previously formed shear band, there is only one likely site for the second shear band to form when indenters with small R_i are employed. This explains the observation of unimodal 3 W distributions of τ_2 for datasets produced by indenters with small R_i (see Fig. 2). Similarly, when indenters with large R_i are used, the second shear band will form near an existing shear band, which has formed along one of the two available trajectories. The difference in the stress to operate shear bands along these trajectories is attributed to the observation of a bimodal 3 W distribution of τ_2 for datasets produced with large R_i. One may then ask, if the paths for forming shear bands are fixed, why is τ_2 not more deterministic, i.e., why are the τ_2 distributions not narrower than those of τ_y? A marginally larger m of τ_2 distributions, compared to that of τ_y, suggests that the stochasticity in strength extends beyond incipient plasticity. The rationale for this is that the shear band cannot be treated as a crack-like defect that operates at a fixed stress governed by the local stress intensity factor. Several studies have shown that the material inside the shear band has a structure that is more disordered than the structure of the surrounding undeformed material, owing to free volume accumulation within it [49,50]. Therefore, the stress required to cause plastic deformation of the material within the shear band will also be governed by the activation of STZs, much like that of the undeformed material. Based on the previous analogy drawn between the 'weakest link' theory and STZ activation, it is expected that τ_2 data would be best described by Weibull distribution.

With an increasing $\dot{P}$, more shear bands nucleate along the D contour (see Fig. 4), which operates at a higher stress, to accommodate the rapidly accumulating strains. This also facilitates the formation of the second shear band along these trajectories, which explains the increasing bimodality of τ_2 distributions at higher $\dot{P}$ (see Fig. 2(a)). Finally, for structurally relaxed samples (SR2 and SR3), the material within the previously formed shear band is in a more structurally relaxed state than that in an as-cast BMG. Therefore, higher stress is required to operate STZs in the previously formed shear band of the relaxed BMG, which explains the shift of τ_2 distributions to higher values (see Fig. 2(c)), much like that seen for τ_y distributions.

5.2. *Shear strength of shear bands*

From the preceding discussion, it is evident that τ_2 data for BMGs, obtained from spherical indenters, corresponds to the stress required to nucleate a fresh shear band along an existing shear band. Recall Eq. (3)-(5), where τ_2 is referred to as the maximum shear stress at which the pop-in occurs. Therefore, τ_2 provides an estimate of the dispersion in the shear strength of a shear band. The strength of the shear band is estimated to be 8–11% lower than the strength of the undeformed BMG, as τ_2 distributions for as-cast BMGs are lower than that of τ_y by the same extent. Similarly, the strength of the shear band in structurally relaxed BMGs is 15–17% lower than that of the undeformed material.

Previously, some studies have estimated the softening of the material inside and around a shear band by different methods [5,51–55]. Bhowmik et al. [53] used the bonded interface technique to measure the hardness of the sub-surface shear band morphology underneath a Vickers indent. They observed that the hardness of the regions with shear bands is 10–16% lower than that of the undeformed BMG, which is similar to what is observed in our study. Bei et al. [56] observed a similar reduction in hardness of the shear banded region in a BMG that was subjected to uniaxial compression. In a follow-up study, Yoo et al. [5], utilizing the same bonded interface method, determined that the reduction in hardness of the shear band compared to that of the undeformed BMG is always ~16–19% irrespective of its structural state. The fact that the results of this study match closely with those in the above-mentioned reports is surprising as they have all been presented with the caveat that the hardness estimates on the shear band is likely to also include contributions from the surrounding undeformed matrix.

Alternately, Pan et al. [52] performed nanoindentation tests directly over shear bands formed on compression samples and observed that their hardness is 36% lower than that of the undeformed BMG. However, their result appears to composition-specific as other shear band characteristics measured by them in their study, such as the shear band thickness, were considerably different than those reported in the literature [31,57,58]. In another study, Nekouie et al. [54] estimated of the hardness of the material inside a shear band by performing hardness tests on fracture surfaces of a 3-point bend-tested BMG, providing the rationale that the fracture surfaces effectively represent the faces of a shear band. They noted that the hardness of the fractured surface is 93% lesser than the hardness of the undeformed BMG. The likely reason for this large discrepancy in the measured strength of the shear band generated during spherical tip indentation and that formed in a 3-point bend fracture test is the difference in the plastic strain accumulated with the shear band. Note that in a 3-point bend test, the shear band within which a crack propagates–leading to failure–accumulates a considerably high plastic strain of ~10% [47,59–67]. This strain is far higher than that accommodated within the first shear band formed under the indenter, which is ~2%. Since larger plastic strains induce greater atomic disorder and increased free volume within the shear band, their strength is also expected to decrease. As a consequence, reduction in the strength of the shear band in the 3-point bend fracture test is higher than that inside a shear band formed during indentation. In essence, results of the present study only provide an estimate of the reduction in the strength of an incipient shear band but not that of mature shear bands that have accumulated large plastic strains.

6. Summary and conclusions

In summary, a detailed statistical analysis of the distribution of the relative stress for post-yield plastic deformation, τ_2, in BMGs reveals that they are best approximated by a three-parameter Weibull distribution. Also, τ_2 distributions have a bimodal nature when higher R_i and higher, $\dot{P}$ or both, were employed. Both these observations are similar to those observed for the distribution of the shear yield strength, τ_y. Moreover, the characteristics of the KDEs of τ_2 and τ_y are similar although the latter is shifted to slightly higher values compared to the former. While the origins of both these distributions were linked to shear band formation, for incipient plasticity, Hertzian contact stress distributions and their gradients determine the stress required to nucleate shear bands along potential trajectories. In contrast, in post yield plasticity, the second shear band prefers to nucleate at an existing shear band, which unexpectedly, does not make the stress distribution more deterministic. This was attributed to the inherent heterogeneity in the strength of the material within the shear bands. On the basis of the relative differences between the KDEs of τ_2 and τ_y, the average shear strength of the shear band in the as cast and structurally relaxed BMGs is estimated as 8–11% and 15–17% of that of the as cast and structurally relaxed BMGs, respectively. These values of the shear band strength match well will other studies in the literature and also provides a guideline for the expected softening in the BMG, once plastic deformation initiates.

Declaration of Competing Interest

The authors declare that they have no known competing financial interests or personal relationships that could have appeared to influence the work reported in this paper.

Acknowledgements

PS and RLN express their gratitude to the Science and Engineering Research Board, Department of Science & Technology (No. SRG/2020/000095), and the Prime Minister Fellowship (PMRF) (No. PMRF/2021/1401226) for supporting this research. UR acknowledges the support by the Structural Metal Alloys Program (Grant reference No.: A18B1b0061) of the Agency for Science, Technology and Research of Singapore.

Supplementary materials

Supplementary material associated with this article can be found, in the online version, at doi:10.1016/j.mtla.2023.101862.

References

[1] S. Nag, R.L. Narayan, J. Jang, C. Mukhopadhyay, U. Ramamurty, Statistical nature of the incipient plasticity in amorphous alloys, Scr. Mater. 187 (2020) 360–365, https://doi.org/10.1016/j.scriptamat.2020.06.045.
[2] J.H. Perepezko, S.D. Imhoff, M.-W. Chen, J.-Q. Wang, S. Gonzalez, Nucleation of shear bands in amorphous alloys, Proc. Natl. Acad. Sci. U.S.A. 111 (2014) 3938–3942, https://doi.org/10.1073/pnas.1321518111.
[3] M. Gao, J.H. Perepezko, Trimodal shear band nucleation distribution in a Gd-based metallic glass via nanoindentation, Mater. Sci. Eng. 801 (2021), 140402, https://doi.org/10.1016/j.msea.2020.140402.
[4] J.Q. Wang, J.H. Perepezko, Focus: nucleation kinetics of shear bands in metallic glass, J. Chem. Phys. 145 (2016), 211803, https://doi.org/10.1063/1.4966662.
[5] B.-G. Yoo, Y.-J. Kim, J.-H. Oh, U. Ramamurty, J. Jang, On the hardness of shear bands in amorphous alloys, Scr. Mater. 61 (2009) 951–954, https://doi.org/10.1016/j.scriptamat.2009.07.037.
[6] B.-G. Yoo, K.-W. Park, J.-C. Lee, U. Ramamurty, J. Jang, Role of free volume in strain softening of as-cast and annealed bulk metallic glass, J. Mater. Res. 24 (2009) 1405–1416, https://doi.org/10.1557/jmr.2009.0167.
[7] C.E. Packard, O. Franke, E.R. Homer, C.A. Schuh, Nanoscale strength distribution in amorphous versus crystalline metals, J. Mater. Res. 25 (2010) 2251–2263, https://doi.org/10.1557/jmr.2010.0299.
[8] I.-C. Choi, Y. Zhao, B.-G. Yoo, Y.-J. Kim, J.-Y. Suh, U. Ramamurty, J. Jang, Estimation of the shear transformation zone size in a bulk metallic glass through statistical analysis of the first pop-in stresses during spherical nanoindentation, Scr. Mater. 66 (2012) 923–926, https://doi.org/10.1016/j.scriptamat.2012.02.032.
[9] I.-C. Choi, Y. Zhao, Y.-J. Kim, B.-G. Yoo, J.-Y. Suh, U. Ramamurty, J. Jang, Indentation size effect and shear transformation zone size in a bulk metallic glass in two different structural states, Acta Mater. 60 (2012) 6862–6868, https://doi.org/10.1016/j.actamat.2012.08.061.
[10] W.L. Johnson, K. Samwer, A universal criterion for plastic yielding of metallic glasses with a (T /Tg) 2 /3 temperature dependence, Phys. Rev. Lett. 95 (2005), 195501, https://doi.org/10.1103/PhysRevLett.95.195501.
[11] F.W. Zok, On weakest link theory and Weibull statistics, J. Am. Ceram. Soc. 100 (2017) 1265–1268, https://doi.org/10.1111/jace.14665.
[12] Y. Sato, S. Shinzato, T. Ohmura, T. Hatano, S. Ogata, Unique universal scaling in nanoindentation pop-ins, Nat. Commun. 11 (2020) 4177, https://doi.org/10.1038/s41467-020-17918-7.
[13] A.G. Perez-Bergquist, H. Bei, K.J. Leonard, Y. Zhang, S.J. Zinkle, Effects of ion irradiation on Zr52.5Cu17.9Ni14.6Al10Ti5 (BAM-11) bulk metallic glass, Intermetallics 53 (2014) 62–66, https://doi.org/10.1016/j.intermet.2014.04.016.
[14] G.R. Garrett, M.D. Demetriou, M.E. Launey, W.L. Johnson, Origin of embrittlement in metallic glasses, Proc. Natl. Acad. Sci. U.S.A. 113 (2016) 10257–10262, https://doi.org/10.1073/pnas.1610920113.
[15] G. Duan, A. Wiest, M.L. Lind, J. Li, W.-K. Rhim, W.L. Johnson, Bulk Metallic Glass with Benchmark Thermoplastic Processability, Adv. Mater. 19 (2007) 4272–4275, https://doi.org/10.1002/adma.200700969.
[16] A.C. Fischer-Cripps, Introduction to Contact Mechanics, Springer US, Boston, MA, 2007, https://doi.org/10.1007/978-0-387-68188-7.
[17] K.L. Johnson, Contact Mechanics, 1st ed., Cambridge University Press, 1985 https://doi.org/10.1017/CBO9781139171731.
[18] C.E. Packard, C.A. Schuh, Initiation of shear bands near a stress concentration in metallic glass, Acta Mater. 55 (2007) 5348–5358, https://doi.org/10.1016/j.actamat.2007.05.054.
[19] P.A. Tobias, D. Trindade, Applied Reliability, 3rd ed., Taylor & Francis, 2011.
[20] J. Sutton, Gibrat's legacy, J. Econ. Lit. 35 (1997) 40–59.
[21] J. Antonaglia, W.J. Wright, X. Gu, R.R. Byer, T.C. Hufnagel, M. LeBlanc, J.T. Uhl, K.a. Dahmen, Bulk Metallic Glasses Deform via Slip Avalanches, Phys. Rev. Lett. 112 (2014) 155501–155505, https://doi.org/10.1103/PhysRevLett.112.155501.
[22] R.V. Hogg, J.W. McKean, A.T. Craig, Introduction to Mathematical Statistics, 8th ed., Pearson, Boston, 2019.
[23] C.R. Rao, Linear Statistical Inference and Its Applications, 2nd ed., Wiley, New York, 2002. Paperback ed.
[24] H. Akaike, A new look at the statistical model identification, IEEE Trans. Automat. Contr. 19 (1974) 716–723, https://doi.org/10.1109/TAC.1974.1100705.
[25] S. Nohut, C. Lu, Fracture statistics of dental ceramics: discrimination of strength distributions, Ceram. Int. 38 (2012) 4979–4990, https://doi.org/10.1016/j.ceramint.2012.02.093.
[26] B.W. Woodruff, A.H. Moore, E.J. Dunne, R. Cortes, A modified Kolmogorov-Smirnov test for weibull distributions with unknown location and scale parameters,

IEEE Trans. Rel. R-32 (1983) 209–213, https://doi.org/10.1109/TR.1983.5221536.
[27] L. Zhang, F. Jiang, Y. Zhao, S. Pan, L. He, J. Sun, Shear band multiplication aided by free volume underthree-point bending, J. Mater. Res. 25 (2010) 283–291, https://doi.org/10.1557/JMR.2010.0028.
[28] B. Moser, J. Kuebler, H. Meinhard, W. Muster, J. Michler, Observation of instabilities during plastic deformation by in-situ SEM indentation experiments, Adv. Eng. Mater. 7 (2005) 388–392, https://doi.org/10.1002/adem.200500049.
[29] T. Rouxel, J. Jang, U. Ramamurty, Indentation of glasses, Prog. Mater Sci. 121 (2021), 100834, https://doi.org/10.1016/j.pmatsci.2021.100834.
[30] D. Tönnies, K. Samwer, P.M. Derlet, C.A. Volkert, R. Maaß, Rate-dependent shear-band initiation in a metallic glass, Appl. Phys. Lett. 106 (2015), 171907, https://doi.org/10.1063/1.4919134.
[31] C. Schuh, T. Hufnagel, U. Ramamurty, Mechanical behavior of amorphous alloys, Acta Mater. 55 (2007) 4067–4109, https://doi.org/10.1016/j.actamat.2007.01.052.
[32] P. Tsai, K. Kranjc, K.M. Flores, Hierarchical heterogeneity and an elastic microstructure observed in a metallic glass alloy, Acta Mater. 139 (2017) 11–20, https://doi.org/10.1016/j.actamat.2017.07.061.
[33] J. Ding, S. Patinet, M.L. Falk, Y. Cheng, E. Ma, Soft spots and their structural signature in a metallic glass, Proc. Natl. Acad. Sci. U.S.A. 111 (2014) 14052–14056, https://doi.org/10.1073/pnas.1412095111.
[34] P. Saini, R.L. Narayan, On simultaneous enhancement in local yield strength and plasticity of short-term annealed bulk metallic glasses, J. Alloys Compd. 898 (2022), 162960, https://doi.org/10.1016/j.jallcom.2021.162960.
[35] A. Jain, Y. Prabhu, D. Gunderov, R.L. Narayan, P. Saini, S. Vincent, P. Sudha, A. D. Bagde, J. Bhatt, Structural characterization, biocorrosion and in-vitro investigation on Zr62Cu22Al10Fe5Dy1 metallic glass for bio-implant applications, J. Non Cryst. Solids 598 (2022), 121928, https://doi.org/10.1016/j.jnoncrysol.2022.121928.
[36] H.-L. Gao, Y. Shen, J. Xu, Weibull analysis of fracture strength for Zr55Ti2Co28Al15 bulk metallic glass: tension–compression asymmetry and porosity effect, J. Mater. Res. 26 (2011) 2087–2097, https://doi.org/10.1557/jmr.2011.210.
[37] J. Zhang, D. Estévez, Y.-Y. Zhao, L. Huo, C. Chang, X. Wang, R.-W. Li, Flexural strength and weibull analysis of bulk metallic glasses, J. Mater. Sci. Technol. 32 (2016) 129–133, https://doi.org/10.1016/j.jmst.2015.12.016.
[38] P.M. Derlet, R. Maaß, The stress statistics of the first pop-in or discrete plastic event in crystal plasticity, J. Appl. Phys. 120 (2016), 225101, https://doi.org/10.1063/1.4971871.
[39] P.M. Derlet, R. Maaß, Critical stress statistics and a fold catastrophe in intermittent crystal plasticity, Phys. Rev. E. 94 (2016), 033001, https://doi.org/10.1103/PhysRevE.94.033001.
[40] P.M. Derlet, R. Maaß, Linking high- and low-temperature plasticity in bulk metallic glasses: thermal activation, extreme value statistics and kinetic freezing, Philos. Mag. 93 (2013) 4232–4263, https://doi.org/10.1080/14786435.2013.826396.
[41] P.M. Derlet, R. Maaß, Linking high- and low-temperature plasticity in bulk metallic glasses II: use of a log-normal barrier energy distribution and a mean-field description of high-temperature plasticity, Philos. Mag. 94 (2014) 2776–2803, https://doi.org/10.1080/14786435.2014.932461.
[42] S.S. Chakravarthy, W.A. Curtin, Stress Gradient Plasticity: concept and Applications, Procedia IUTAM. 10 (2014) 453–461. doi:10.1016/j.piutam.2014.01.040.
[43] S.S. Chakravarthy, W. a Curtin, Stress-gradient plasticity, Proc. Natl. Acad. Sci. U.S.A. 108 (2011) 15716–15720, https://doi.org/10.1073/pnas.1107035108.
[44] D. Liu, Y. He, B. Zhang, L. Shen, A continuum theory of stress gradient plasticity based on the dislocation pile-up model, Acta Mater. 80 (2014) 350–364, https://doi.org/10.1016/j.actamat.2014.07.043.
[45] U. Ramamurty, M.L. Lee, J. Basu, Y. Li, Embrittlement of a bulk metallic glass due to low - temperature annealing, Scr. Mater. 47 (2002) 107–111.
[46] P. Murali, U. Ramamurty, Embrittlement of a bulk metallic glass due to sub-Tg annealing, Acta Mater. 53 (2005) 1467–1478, https://doi.org/10.1016/j.actamat.2004.11.040.
[47] R.L. Narayan, D. Raut, U. Ramamurty, A quantitative connection between shear band mediated plasticity and fracture initiation toughness of metallic glasses, Acta Mater. 150 (2018) 69–77, https://doi.org/10.1016/J.ACTAMAT.2018.03.011.
[48] F.H. Dalla Torre, D. Klaumünzer, R. Maaß, J.F. Löffler, Stick–slip behavior of serrated flow during inhomogeneous deformation of bulk metallic glasses, Acta Mater. 58 (2010) 3742–3750, https://doi.org/10.1016/j.actamat.2010.03.011.
[49] A.L. Greer, Y.Q. Cheng, E. Ma, Shear bands in metallic glasses, Mater. Sci. Eng. 74 (2013) 71–132, https://doi.org/10.1016/j.mser.2013.04.001.
[50] M. Wakeda, Y. Shibutani, S. Ogata, J. Park, Relationship between local geometrical factors and mechanical properties for Cu–Zr amorphous alloys, Intermetallics 15 (2007) 139–144, https://doi.org/10.1016/j.intermet.2006.04.002.
[51] S. Xie, E.P. George, Hardness and shear band evolution in bulk metallic glasses after plastic deformation and annealing, Acta Mater. 56 (2008) 5202–5213, https://doi.org/10.1016/j.actamat.2008.07.009.
[52] J. Pan, Q. Chen, L. Liu, Y. Li, Softening and dilatation in a single shear band, Acta Mater. 59 (2011) 5146–5158, https://doi.org/10.1016/j.actamat.2011.04.047.
[53] R. Bhowmick, R. Raghavan, K. Chattopadhyay, U. Ramamurty, Plastic flow softening in a bulk metallic glass, Acta Mater. 54 (2006) 4221–4228, https://doi.org/10.1016/j.actamat.2006.05.011.
[54] V. Nekouie, S. Doak, A. Roy, U. Kühn, V.V. Silberschmidt, Experimental studies of shear bands in Zr-Cu metallic glass, J Non Cryst Solids 484 (2018) 40–48, https://doi.org/10.1016/j.jnoncrysol.2018.01.009.
[55] U. Ramamurty, S. Jana, Y. Kawamura, K. Chattopadhyay, Hardness and plastic deformation in a bulk metallic glass, Acta Mater. 53 (2005) 705–717, https://doi.org/10.1016/j.actamat.2004.10.023.
[56] H. Bei, S. Xie, E.P. George, Softening Caused by Profuse Shear Banding in a Bulk Metallic Glass, Phys. Rev. Lett. 96 (2006), 105503, https://doi.org/10.1103/PhysRevLett.96.105503.
[57] V.K. Sethi, R. Gibala, A.H. Heuer, Transmission electron microscopy of shear bands in amorphous metallic alloys, Scr. Metall. 12 (1978) 207–209, https://doi.org/10.1016/0036-9748(78)90165-5.
[58] T. Masumoto, H. Kimura, A. Inoue, Y. Waseda, Structural stability of amorphous metals, Mater. Sci. Eng. 23 (1976) 141–144, https://doi.org/10.1016/0025-5416(76)90183-X.
[59] D. Raut, R.L. Narayan, P. Tandaiya, U. Ramamurty, Temperature-dependence of mode I fracture toughness of a bulk metallic glass, Acta Mater. 144 (2018) 325–336, https://doi.org/10.1016/j.actamat.2017.10.063.
[60] C. Wang, Q.P. Cao, X.D. Wang, D.X. Zhang, U. Ramamurty, R.L. Narayan, J.-Z. Jiang, Intermediate temperature brittleness in metallic glasses, Adv. Mater. 29 (2017), 1605537, https://doi.org/10.1002/adma.201605537.
[61] R.L. Narayan, P. Tandaiya, R. Narasimhan, U. Ramamurty, Wallner lines, crack velocity and mechanisms of crack nucleation and growth in a brittle bulk metallic glass, Acta Mater. 80 (2014) 407–420, https://doi.org/10.1016/j.actamat.2014.07.024.
[62] R. Narasimhan, P. Tandaiya, I. Singh, R.L. Narayan, U. Ramamurty, Fracture in metallic glasses: mechanics and mechanisms, Int. J. Fract. 191 (2015) 53–75, https://doi.org/10.1007/s10704-015-9995-3.
[63] R.L. Narayan, P. Tandaiya, G.R. Garrett, M.D. Demetriou, U. Ramamurty, On the variability in fracture toughness of 'ductile' bulk metallic glasses, Scr. Mater. 102 (2015) 75–78, https://doi.org/10.1016/j.scriptamat.2015.02.017.
[64] R.L. Narayan, L. Tian, D. Zhang, M. Dao, Z.-W. Shan, K.J. Hsia, Effects of notches on the deformation behavior of submicron sized metallic glasses: insights from in situ experiments, Acta Mater. 154 (2018) 172–181, https://doi.org/10.1016/j.actamat.2018.05.041.
[65] D. Raut, R.L. Narayan, Y. Yokoyama, P. Tandaiya, U. Ramamurty, Fracture of notched ductile bulk metallic glass bars subjected to tension-torsion: experiments and simulations, Acta Mater. 168 (2019) 309–320, https://doi.org/10.1016/j.actamat.2019.02.025.
[66] C. Chen, M. Gao, C. Wang, W.-H. Wang, T.-C. Wang, Fracture behaviors under pure shear loading in bulk metallic glasses, Sci. Rep. 6 (2016) 39522, https://doi.org/10.1038/srep39522.
[67] P. Tandaiya, R. Narasimhan, U. Ramamurty, Mode I crack tip fields in amorphous materials with application to metallic glasses, Acta Mater. 55 (2007) 6541–6552, https://doi.org/10.1016/j.actamat.2007.08.017.